Acta Montanistica Slovaca
ISSN 1335-1788
actamont.tuke.sk

The synthesis of biographene oxide from the graphitic structure of PKS, EFB and OPF

Noor H. JABARULLAH[1], Rapidah OTHMAN[2], Afiqah Samsul KAMAL[2], Marmy Roshaidah Mohd SALLEH[2], Mariusz URBAŃSKI[3] and Wiesław LISZEWSKI[3]*

Authors' affiliations and addresses:
[1] Malaysian Institute of Aviation Technology, Universiti Kuala Lumpur, Sepang 43900, Malaysia
e-mail: nhafidzah@unikl.edu.my

[2] Chemical Engineering Section, Malaysian Institute of Chemical and Bioengineering, Universiti Kuala
Lumpur, Melaka 78000, Malaysia
e-mail: afiqah.samsul30@s.unikl.edu.my
e-mail: rapidah@unikl.edu.my
e-mail: marmy@unikl.edu.my

[3] Road and Bridge Research Institute, Instytutowa 1, 03-302 Warsaw, Poland
e-mail: murbański@ibdim.edu.pl
e-mail: wliszewski@ibdim.edu.pl

***Correspondence:**
Noor Hafidzah Jabarullah, Malaysian Institute of Aviation Technology, Universiti Kuala Lumpur, Sepang 43900, Malaysia
e-mail: nhafidzah@unikl.edu.my

How to cite this article:
Jabarullah, N.H., Othman, R., Kamal, A.S., Mohd Salleh, M.R., Urbański, M. and Liszewski, W. (2022). The synthesis of biographene oxide from the graphitic structure of PKS, EFB and OPF. *Acta Montanistica Slovaca*, Volume 27 (4), 864-875.

DOI:
https://doi.org/10.46544/AMS.v27i4.03

Abstract
The increasing global demand for graphite and environmental issues due to the extraction of natural graphite has become motivations to improve the process development of synthetic graphite. However, the conventional process for synthetic graphite production requires high temperatures, extreme process conditions, and expensive equipment. This drives further research work on finding more straightforward options. This research study a simpler direct transformation method using Palm Kernel Shell (PKS), Oil Palm Fond (OPF, Empty Fruit Bunch (EFB) as carbon precursors via a catalytic graphitization process. The process involved raw material preparation, carbonization process, Iron-Silica catalyst impregnation and graphitization. Three parameters were observed, including graphitization temperature, type of raw material and amount of Iron catalyst loadings. The Bio-synthetic graphite produced were later undergone an "improved method" to form Graphene Oxide (GO). The graphitic carbon produced was characterized using X-Ray Diffraction (XRD) and Raman spectroscopy, Brunauer-Emmet-Teller (BET) Surface Area and High-Resolution Transmission Electron Microscope (HRTEM). Overall successful transformation of amorphous carbon to graphitic structure for PKS, EFB, and OPF was evidenced by the XRD pattern and Raman spectra. It was found that PKS was the greatest carbon precursor for the graphitization process, followed by EFB and OPF. The former exhibited the nearest interlayer spacing to natural graphite with the lowest Id/Ig value. This can be seen from the HRTEM image of the PKS-1300-40 sample. The results attributed to the highest percentage of lignin in PKS rather than in EFB and OPF. A very significant transformation of bio-synthetic graphite to GO powder was also evidenced in XRD patterns and RAMAN spectroscopy. As for bio-synthetic graphene PKS, EFB and OPF depicted XRD patterns with broad peak centring around 2θ~25°. It was found an absence of GO characteristic peak at 2θ~10.7°.

Keywords
Graphene Oxide, Graphitization, Carbonization, Graphite, Biomass, Impregnation.

Introduction

Agricultural and food waste biomass, including coconut shell, oil palm biomass, orange peel, and sugarcane bagasse, have all recently garnered global interest as a potential low-cost feedstock for producing nanomaterials (Mohammed Abdillah & Yoshito, 2022; Plewa, 2019). Biomass is plant material such as trees, grass, agricultural crops or biological material. It can be used as a solid fuel and can be converted to liquid or gaseous form for use in the production of electricity, heat, chemicals or fuel (Kamil et al., 2006). Palm oil biomass waste has been produced during fresh fruit bunch processing, replanting and pruning (Mohammad Padzil et al., 2020). Generally, the waste can be classified into Empty Fruit bunch (EFB), Palm Oil Mill Effluent (POME), Mesocarp Fibre, Palm Kernel shell (PKS), Palm Kernel Cake, and Oil Palm Trunks (Dalton et al., 2017), (King, 2006). The growth of waste concerns as it is harmfully related to environmental pollution issues. Due to low ash and high carbon content, biomass was utilized for soil amendment, energy generation, biofuel, and filler material (Kaniapan et al., 2021; Srinivasan et al., 2015). These lignocellulosic biomasses are natural, non-toxic, abundant, sustainable, and renewable materials, promoting the potential of lignocellulosic material for numerous advanced applications. Therefore, maximizing the usage of palm oil byproducts help in economic growth and reduce dependency on fossil fuel and produce more job opportunities in agriculture, forest management, oil and chemical industry (Mohd et al., 2020; Serrano-Ruiz et al., 2010).

Lignocellulosic biomass is an attractive resource for advanced material synthesis as it is carbon-rich, omnipresent, environmentally benign and low-cost (Hoekstra et al., 2015). Hence, biomass waste is a promising carbon feedstock for graphite production (Liu et al., 2018). Biomass is composed of three main fractions, namely, cellulose, hemicellulose, and lignin, which contain abundant polar hydroxyl and carbonyl groups (Bernd et al., 2017; Wang et al., 2013). An important factor that influenced the degree of graphitization is the chemical composition of its carbon sources. The selection of plant-based biomass with high lignin fraction, low cellulose fraction, low oxygen and high nitrogen content is important to produce highly graphitic carbon, controllable defect and good conductivity (Yang Liu et al., 2018). Graphitization is a transformation process into a graphitic structure involving a heat treatment process. The process of graphitization involves limited movements and rearrangement of carbon atoms, which undergo a reconstructive transformation during heat treatment (Kim et al., 2016; Tamashausky, 2006).

Many researchers have investigated different raw materials such as sawdust, corn stalk, green tea waste, coconut coir and coconut stalk waste as raw material in graphitic carbon production (Sankar et al., 2019), (Xia et al., 2018). Graphite is a natural mineral composed of carbon (Hobart, 2015). Natural occurrences of graphite are classified into a few categories magmatic, regional, hydrothermal and meteoric (King, 2006). This research focuses on synthesizing biographene oxide by utilizing new raw materials Palm Kernel Shell, Empty Fruit Bunch and Oil Palm Frond with the impregnation of Iron-Silica hybrid catalysts as a new promising pathway for future large-scale production and catalytic graphitization at different heat treatment temperatures.

Several methods are used to delaminate graphite. The method used is the oxidation of graphite to graphite oxide, exfoliation process to graphene oxide and followed by thermal or chemical reduction to produce reduced graphene oxide (Salvador et al., 2019). The heating and processing of materials using microwaves have become increasingly popular for industrial applications. Microwave processing can rapidly produce materials with unique properties and reductions in manufacturing costs and processing times (Ingrid et al., 2000). Microwave heating has been proven suitable for synthesizing and functionalizing nanotubes and nanofibers due to its potential to reduce time significantly, cost and the number of steps required compared to conventional approaches. A microwave reactor for expanded graphite production has been patented, and Mitsubishi Heavy Industries Ltd. claimed to successfully produce graphite materials through microwave heating (Zoraida et al., 2021). Microwave heating of a material depends to a large extent on its dissipation factor, which is the loss ratio or dielectric loss factor to the dielectric constant of the material. Microwave heating requires the conversion of electrical energy to heat energy to raise the temperature of the material (Lovas et al., 2011). Graphene oxide is graphite that has been oxidized to intersperse carbon layers with oxygen molecules and reduced to completely separate the carbon layers into individual or multiple layers of graphene. The first attempt to synthesize graphite oxide was performed in 1859 by British chemist B. C. Brodie who investigated the reactivity of flake graphite. It is a chlorate route, where potassium chlorate is used as an oxidizing agent. Benjamin Brodie treated graphite with a number of strong oxidizing agents for the first time to decode its structure (Adela et al., 2022). Graphene oxide is effectively a byproduct of this oxidation because when the oxidizing agent reacts with the graphite, the interplanar spacing between the graphite layers increases. The fully oxidized compound can then be dispersed in a basic solution such as water, and graphene oxide is then produced (Paulchamy et al.,2015). Recent methods of making GO are based on the significant ability of layered graphite for intercalation. It allows active metal atoms and some types of oxidizing agents to penetrate between the flat carbon layers of crystalline graphite, increasing the distance between the layers and modifying the surface of the layers by chemically bonded functional groups. Finally, the action of a suitable oxidizing agent causes a complete disintegration of the graphite crystal into a separate carbon monolayer with a chemically modified surface (Artur & Alexander, 2019). High-quality graphene oxide nanoplatelets were

reported to have been synthesized using biochar derived from rice straw biomass, an agricultural waste product of large-scale production (Mohammed Abdillah & Yoshito, 2022; Mate et al., 2017).

Materials and methods

Carbonization

The raw PKS, EFB and OPF in powdered form were carbonized under nitrogen flow to remove volatile matter and prevent the combustion process during carbonization (Yan et al., 2018). The 4g of every sample was carbonized using Carbolite 1800C Tube Furnace / Model CTF 18/300. The carbonization temperature was performed at 500℃ over 2 hours by heating up at the ramping rate of 5℃/min and under 30 ml/min nitrogen flow. Carbonized samples were allowed to cool down naturally to room temperature.

Impregnation of catalyst

Iron(III) nitrate nanohydrate was dissolved in 100 ml of distilled water. 5g of the carbonized carbon (PKS-CARBON/EFB-CARBON/OPF-CARBON) was weighed and added under vigorous stirring (Nettelroth et al., 2016). It was then transferred to a round bottom flask and refluxed for 5 hours. Next, the sample was filtered using filter paper and dried for 24 hours in the drying oven. The sample of 2 grams was weighed and placed in a quartz boat on top of SiO2 nanoparticles (Libo, 2014). The details of the amount of catalyst loading (wt.%) are summarized in Table 1 below. The amount of silica was kept constant for each sample. Control samples were prepared from each raw material without the addition of Iron (III) Nitrate 0 wt.%.

Tab.1. The amount of catalyst loading (wt.%) in gram

Amount of Iron (III) Nitrate	Amount of SiO_2 nanoparticle
80wt.% (17.319g)	0.4g
60wt.% (12.98g)	0.4g
40 wt.% (8.66g)	0.4g
20 wt.% (4.3294g)	0.4g
0 wt.% (0 g)	0.4g

Graphitization process

The 2g of all impregnated catalyst samples were placed in a quartz boat and inserted into Carbolite 1800C Tube Furnace / Model CTF 18/300. The graphitization parameter was carried out at temperatures ranging from 1000℃ to 1400 ℃ over 2 hours at a ramping rate of 5℃/min and under 30 ml/min nitrogen flow. Graphitized samples were allowed to cool down naturally to room temperature. The effect of catalyst loading was observed by using 5 different amounts of catalyst loading ranging from 0%-80%. The details of the amount of catalyst loading (wt.%) are summarized in Table 1 above. The samples were then graphitized at 1000℃, 1100℃, 1200℃, 1300℃ and 1400℃ to study the effect of graphitization temperature on bio-graphite produced. For sample prepared using PKS at 1000℃ graphitization temperature and 80% Iron loading was denoted as PKS-1000-80 in the order of raw material-temperature-percentage of catalyst loading. After the graphitization process, the sample underwent an acid-washing procedure. 2 grams of each Bio-synthetic graphite were stirred with 1 mol HCl for 24 hours for catalyst removal. The samples were washed with deionized water and then oven dried at 80℃ overnight prior to air storage.

Synthesis of Biographene Oxide

The method previously used by Marcano et al. (2010), Nasir et al. (2017) and a combination from (Zaaba et al., 2017) was applied in this research work to produce graphene oxide (GO). The selection is based on the findings that GO produced using this method does not involve a large exothermic reaction, produces no toxic gas, improved yields and a higher fraction of well-oxidized hydrophilic carbon material was obtained (Marcano et al., 2010). The 360 ml of sulfuric acid (H_2SO_4) and 40 ml of phosphoric acid H_3PO_4 in a volume ratio of 9:1 was mixed and stirred for several minutes. Then, 3 grams of graphite powder and 18 grams of Potassium permanganate KMnO4 were added into the mixing solution under stirring conditions resulting in slightly exothermic conditions around 40 °C. The mixture was then heated to 50 °C and stirred for 12 hours until the solution became dark green. The reaction was then cooled down to room temperature and poured into ice (400mL).

To eliminate excess $KMnO_4$, 3 ml of hydrogen peroxide H_2O_2 (30 wt.%, aq.) was dropped slowly and stirred for 10 minutes. As an exothermic reaction occurred, the mixture was cool down. The mixture was sifted through a $206\mu m$ metal sieve and filtered. The filtrate was then centrifuged using Eppendorf Centrifuge 5430R at 5000 rpm for 7 minutes, and the supernatant was decanted away. The remaining solid material was then washed in succession with 200 ml of water and 200 mL of 30% HCl. Then, the sample was rewashed 3 times again. The

washed GO powder was then dried in the oven at 90℃ for 24 hours and was named GO raw material- temperature-percentage of catalyst loading.

The GO produced then undergoes analysis using X-ray diffraction (XRD) analysis, Raman spectroscopy analysis, Brunauer-Emmet- Teller (BET) for the pore structure, and pore size and surface area analysis. A High-Resolution transmission electron microscope (HRTEM) is used to produce an image of material at an atomic level to determine thickness, number of layers and cross-sectional view of bio-graphene. This is to determine and compare transformation changes between bio-synthetic graphite and bio-graphene structure.

Results

Overall, it can be observed that the most intense and sharp peak was presented by the EFB-1300-60, corresponding to the highest degree of graphitization. This suggested that the optimum conditions for EFB material were at temperature 1300ºC and 60 wt.% catalyst loading. However, a few more EFB samples showed some degree of graphitization, including EFB-1400-60, EFB-1200-40, and EFB-1200-80.

Of all PKS samples, few samples showed successful transformation to a well-organized structure as significant intensified graphite peaks were clearly observed. These include PKS-1300-20, PKS-1300-40, PKS-1100-80, and PKS-1400- 60. Nevertheless, it can be deduced that the optimum conditions for PKS material were defined at 20 wt.% catalyst loading and temperature 1300℃. Overall, the optimum conditions for OPF material were at a catalyst loading of 40% and a heat treatment temperature of 1300°C. However, a few samples showed highly ordered carbon structures that can be identified, including OPF-1100-80, OPF-1300-40, OPF-1100-20, OPF-1300-60, and OPF-1200-60. Referring to XRD patterns for EFB and PKS, which can be seen in Figure 1(a-e) and Figure 2 (a-e) and Figure 3(a-e), respectively, the heat treatment temperature at 1300℃ was the most favourable.

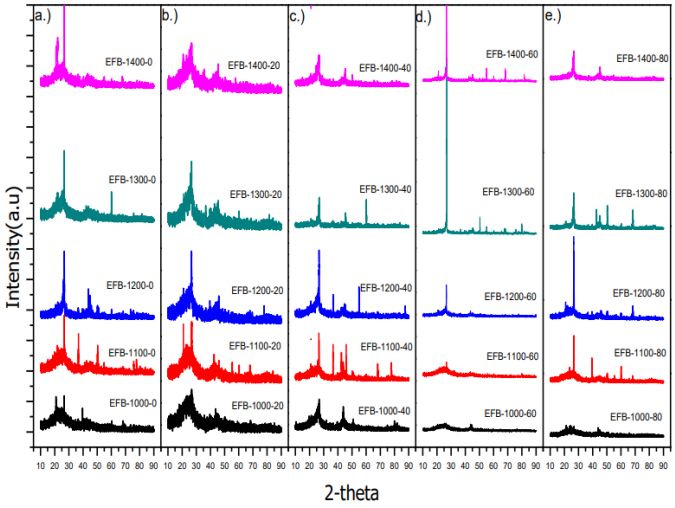

Fig. 1. XRD pattern for EFB samples prepared at various temperatures and at a) 0% Iron catalyst, b) 20% Iron catalyst, c) 40% Iron catalyst, d) 60% Iron catalyst, e) 80% Iron catalyst loading.

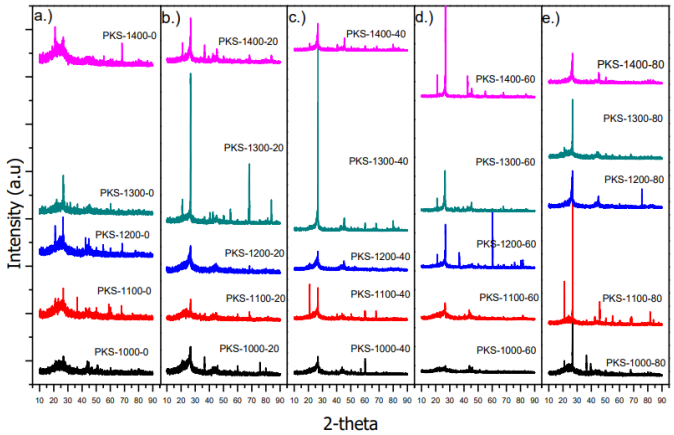

Fig. 2. XRD pattern for PKS samples prepared at various temperatures and at a) 0% Iron catalyst, b) 20% Iron catalyst, c) 40% Iron catalyst, d) 60% Iron catalyst, e) 80% Iron catalyst loading.

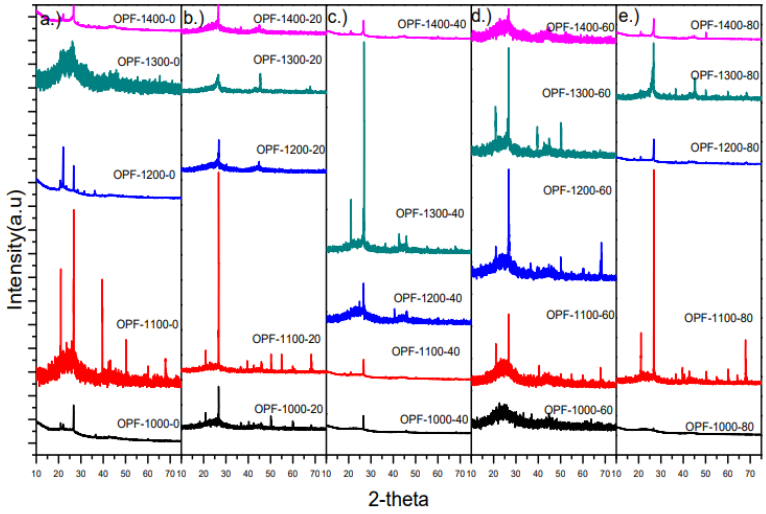

Fig. 3. XRD pattern for OPF samples prepared at various temperatures and at a) 0% Iron catalyst, b) 20% Iron catalyst, c) 40% Iron catalyst, d) 60% Iron catalyst, e) 80% Iron catalyst loading.

All the samples that displayed a distinctive and obvious sharp peak from Table 2 were further investigated and compared, as shown in Figure 4.7. The XRD patterns for the selected sample were plotted for further discussion.

Tab. 2. List of samples with significant intensified graphite peak based on graphitization temperature parameter and wt.% of catalyst loading.

Raw material	EFB	PKS	OPF
Sample name	EFB-1300-60	PKS-1300-20	OPF-1100-80
	EFB-1400-60	PKS-1300-40	OPF-1300-40
	EFB-1200-40	PKS-1100-80	OPF-1100-20
	EFB-1200-80	PKS-1400-6	

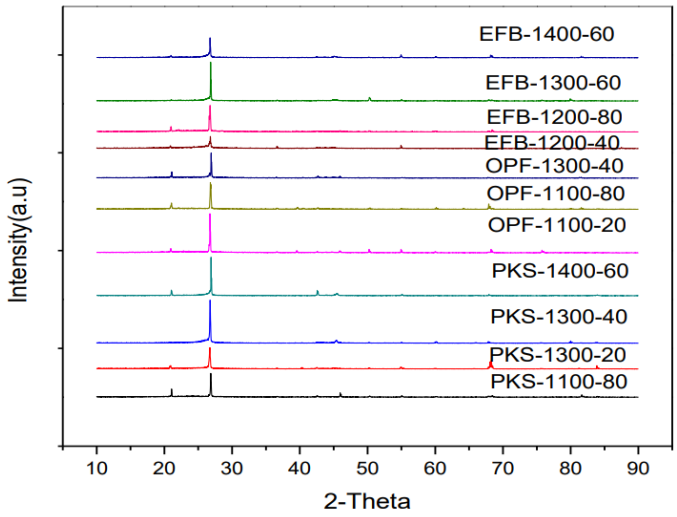

Fig. 4. Comparison of the sample with the highest degree of graphitization

Generally, all selected samples showed an insignificant broad hump at around 2θ =20°- 30° related to the minimal existence of amorphous structure, indicating successful transformation to highly graphitic was achieved. It can be observed that the PKS sample showed the highest intensified peak, followed by EFB and OPF. To further confirm which raw biomass material was successfully transformed into a highly graphitic structure, an interlayer spacing d*002* was calculated according to Bragg's equation (1), as tabulated in Table 3 below (Qiu et al., 2019).

$$d002=\lambda 2sin\theta(002) \quad (1)$$

Where λ is the X-ray wavelength and θ is the 002-surface diffraction angle. The value of d*002* spacing was seen to be in the range between 0.3315 - 0.3335 nm, close to the value of commercial graphite tested (0.3347 nm) and less than 0.344 nm for disordered carbon material.

Tab. 3. Physical properties of selected bio-graphitic carbon

Sample name	d-spacing	Lc 002	La	Id/Ig
OPF 1100-20	0.3335	108.74	73.79	0.93
EFB 1300-60	0.3333	72.46	36.90	0.47
PKS 1300-40	0.3332	62.10	73.77	0.46
PKS 1300-20	0.3331	72.46	18.47	1.02
EFB 1200-80	0.3330	145.06	63.74	0.48
EFB 1200-40	0.3328	41.81	85.16	0.98
EFB 1400-60	0.3323	108.76	18.47	0.55
PKS 1100-80	0.3321	72.48	88.57	0.99
OPF 1100-80	0.3319	54.38	110.78	0.99
PKS 1400-60	0.3316	106.95	88.58	0.69
OPF 1300-40	0.3315	87.00	295.53	0.98

Of all catalysts, OPF-1100-20, EFB-1300-60, and PKS-1300-40 samples showed the nearest interlayer spacing value to 0.3347 nm, which corresponds to commercial graphite, suggesting that the ordered carbon framework was successfully achieved. The d*002* value obtained from this study proved that the structure of all selected samples was successfully modified and transformed into the graphitic domain. Since OPF-1100-20, EFB-1300-60, and PKS-1300-40 had been proven to achieve a high degree of graphitization by the calculation from the interlayer spacing data (*d002*), the XRD profiles for the three distinctive samples were plotted and compared with biomass materials before graphitization (biochar EFB carbon, OPF carbon and PKS carbon), commercial graphite and noncatalytic sample (sample prepared without catalyst) in order to observe the significant transformation. The comparison can be seen in Figure 5.

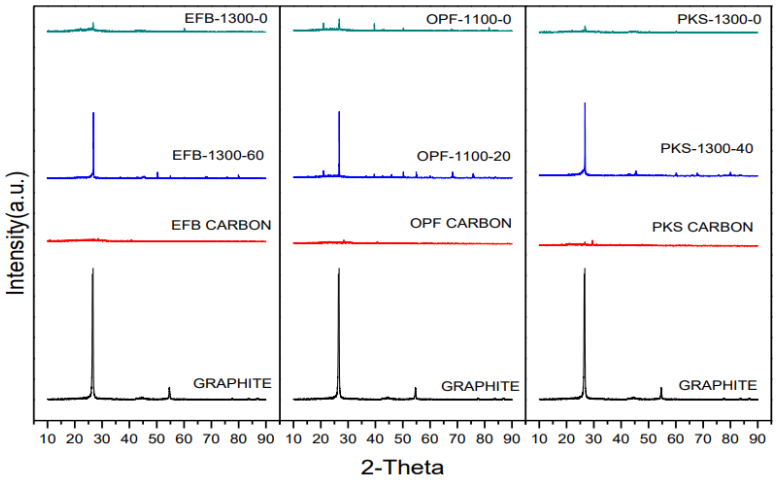

Fig. 5. Comparison of EFB-1300-60, OPF-1100-20 and PKS-1300-40 with commercial graphite, biochar and noncatalytic carbon

As expected, biochar samples (EFB, PKS and OPF carbon) revealed almost no diffraction peak, while the sample prepared without catalyst (EFB-1300-0, OPF-1100-0, and PKS-1300-0) exhibited only a small amount of characteristic peak. The results suggested that the structure was still in an amorphous framework. In contrast, Iron-Silica catalyzed carbon showed a very intensified graphite peak. The EFB-1300-60, OPF- 1100-20 and PKS-1300-40 showed XRD peaks at $2\theta\sim$ 26°,44°,54°,78°, which were assigned to the (002), (101), (004) and (110) diffraction of the graphitic framework.

The nature of the graphitization of carbon was further evaluated by Raman spectroscopy. Raman spectra for carbon materials consist of four first-order Raman bands, each from different vibratory modes. For graphitic carbon material, the most significant bands were located near 1580 cm^{-1}, representing vibration in the ideal graphite lattice(G) band (Johnson & Faber, 2011; Kim et al., 2016; Lim et al., 2017). Meanwhile (D) band appear as increasing in structural defect; D1 (1350cm^{-1}), D2 (1700 cm^{-1}), and D3(1400 cm^{-1}) bands represent vibrations from graphene layer edges, surfaces, and amorphous regions, respectively (Major et al., 2018).

The peak intensity ratio of prominent G and D1 bands indicates the degree of graphitic material content and quality (Johnson & Faber, 2011). The relative intensity ratio between D and G bands (Id/Ig) reflects the degree of graphitization. A low Id/Ig value indicates a high degree of graphitization (Sevilla et al., 2007). The Raman spectra for the sample from Table 2 were portrayed in Figure 6 below, while Id/Ig values were summarized in Table 3 above.

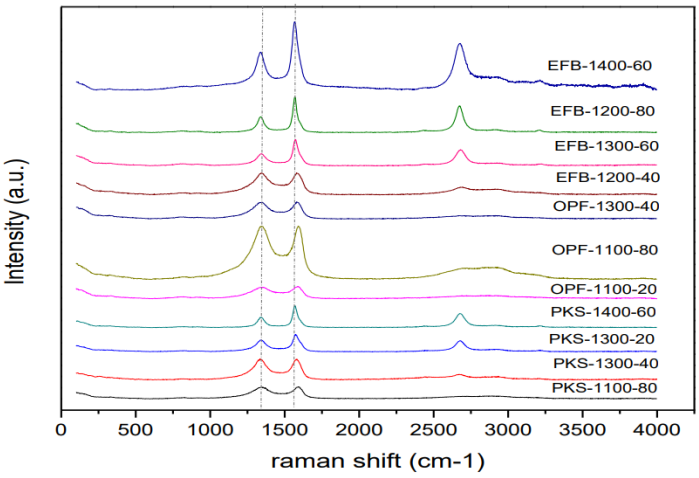

Fig. 6. Raman spectra for all samples with the highest degree of graphitization

Figure 6 shows Raman spectroscopy of all samples with a high degree of graphitization based on XRD profiles observed from various heat treatment temperatures and catalyst loadings. Generally, all samples showed a higher G-band peak of 1580 $cm^{-1,}$ giving a general view that the sample was successfully graphitized. However, to further compare defect structure, the Id/Ig ratio was calculated and summarized in Table 3. The Id/Ig ranged from 0.46 - 1.02, showing that the structure for samples with lower values was more well-ordered as the defect vibration due to the amorphous surface or another defect is lower. To simplify this, the sample with lower Id/Ig value from each raw material tabulated in Table 4 was selected and compared with commercialized graphite, as shown in Figure 7, to better understand the different types of raw material.

Tab. 4. Sample with lower Id/Ig value for each raw material

Raw material	Sample name	I_d/I_g
EFB	EFB-1300-60	0.47
PKS	PKS-1300-40	0.46
OPF	OPF-1100-20	0.93

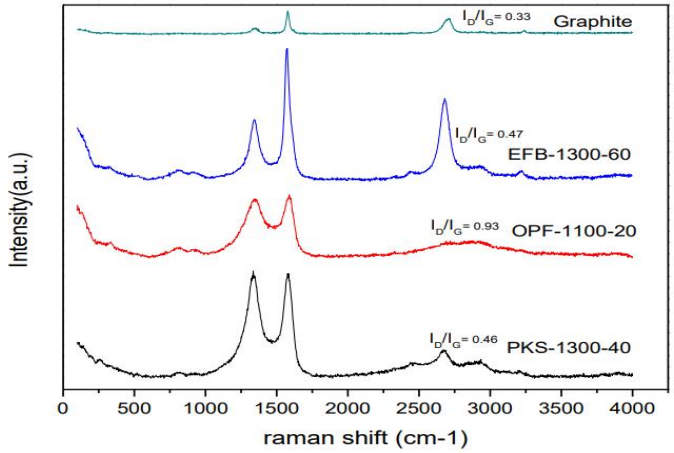

Fig. 7. Raman spectra for sample OPF-1100-20, EFB-1300-60, and PKS-1300- 40

From Figure 7, the Id/Ig values for OPF-1100-20, EFB-1300-60, PKS-1300-40 and commercial graphite are 0.93,0.47,0.46 and 0.33, respectively. The low relative intensity ratio of Id/Ig proves that successful alteration of amorphous material has been achieved with an Iron-Silica catalyst. Therefore, the sample from PKS material showed high crystallinity and low defect, as the Id/Ig ratio for PKS is lower than EFB and OPF. This Raman result is coherent with the XRD finding in which, based on peak intensity, the degree of graphitization for all materials

is in the order of PKS > EFB > OPF. This result suggests that the great performance for the raw biomass material is in the order of PKS > EFB > OPF. As these three samples have been successfully transformed into the graphitic structures, they are denoted as bio-synthetic graphite. Nitrogen adsorption-desorption isotherms were also measured to investigate further the Brunauer-Emmet-Teller (BET) surface area for samples listed in Table 4. The N_2 adsorption-desorption isotherms of PKS-1300-40, OPF-1100-20 and EFB-1300-60 are shown in Figure 8, and the BET surface area of the samples is summarized in Table 5.

Tab.5. Pore parameter of bio-graphite

Bio-graphite sample	S_{BET} m^2 /g	Pore volume cm^3 /g	Pore size (width) nm
PKS-1300-40	139.03	0.144	4.13
EFB-1300-60	197.42	0.272	5.51
OPF-1100-20	287.85	0.214	2.98

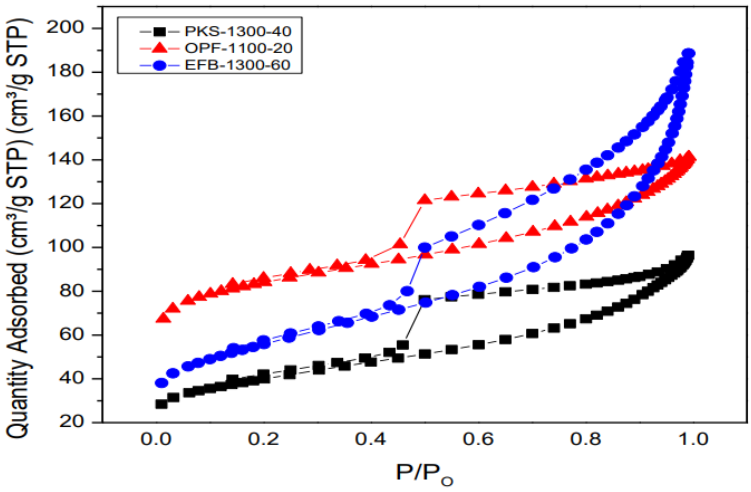

Fig. 8. Nitrogen adsorption isotherms of bio-synthetic graphite

From Table 5, the BET surface area of the sample prepared from different raw biomass material was in the range between 139.03 - 287.85 m^2/g and in the order of OPF > EFB > PKS. It can be deduced that PKS-1300-40 had achieved the highest degree of graphitization, and this was evidenced by the lowest BET surface area obtained from the N_2 adsorption. Thus, the degree of graphitization is inversely proportional to the SBET surface area.

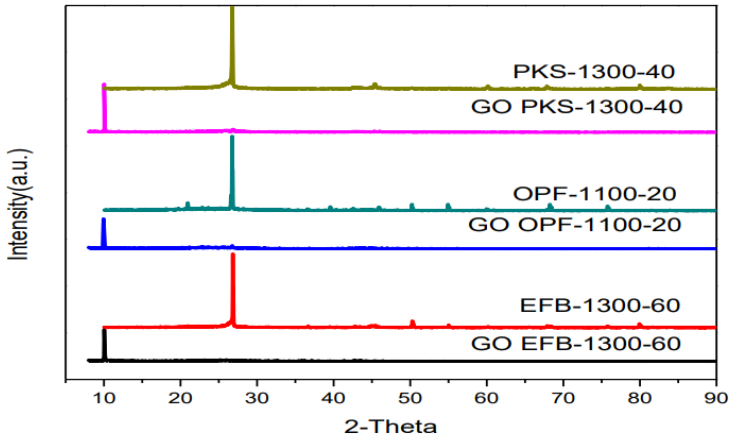

Fig. 9. Comparison between GO and bio-synthetic graphite

After the oxidation process, the graphite peak gradually disappears while a new peak appears at a lower angle 2θ~$10° - 11°$, which refers to the interlayer spacing of 0.857 nm. The GO sample shows a characteristic peak corresponding to (001) appearing at a lower angle due to the intercalation of the oxygen functional group on the

basal plane of the GO sheet (Khosroshahi et al., 2018). The peak is not as sharp as the Graphite peak due to the deterioration of crystal structure, and the position of the GO peak mainly depends on the degree of oxidation of graphite (De Silva et al., 2018). A higher interlayer spacing of GO indicates a higher order of oxidation and exfoliation (De Silva et al., 2018). The XRD patterns of GO were in the absence of 2θ~26°(002) peak, proving that complete oxidation had occurred (Poh et al., 2012). For each GO material prepared from GO PKS-1300-40, GO OPF-1100-20, and GO EFB-1300-60 showed the disappearance of 2θ~26°(002) peaks suggesting raw materials were successfully oxidized. During the oxidation of graphite to graphene oxide (GO) via the Improved method, the presence of strong oxidants and strong acids resulted in the oxygen groups such as hydroxyl (-OH) or epoxide (-O-) group introduced and attached to a significant fraction of carbon atoms at which the sp2 bonded structure of the stacked graphene sheets have been broken in the basal lane (Abdolhosseinzadeh et al., 2015). This process changes the hybridization of an oxidized carbon atom from sp2 to tetrahedral sp3 (Mcallister et al., 2007). It causes defects resulting in increases of d-spacing between the layers.

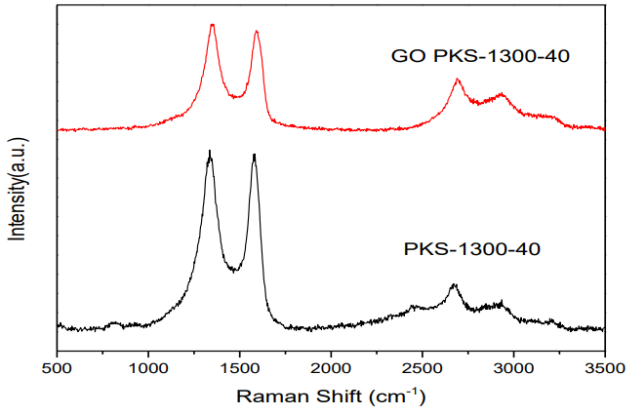

Fig. 10.Raman spectra of bio-graphite and GO from PKS-1300-40.

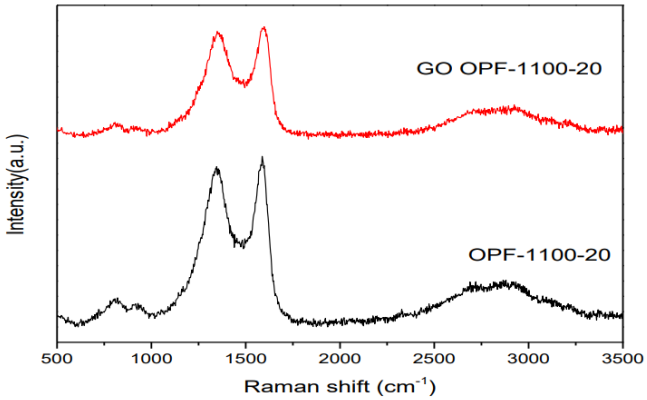

Fig. 11. Raman spectra of bio-graphite and GO from OPF-1100-20.

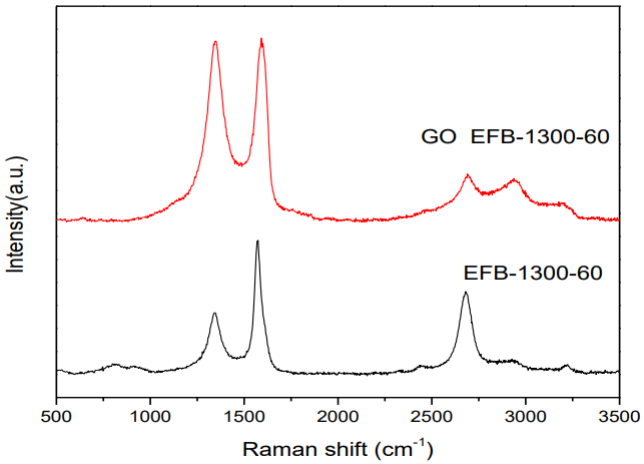

Fig. 12. Raman spectra of bio-graphite and GO from EFB-1300-60.

Figure 10 shows the Raman spectra of GO and Bio-synthetic graphite from PKS-1300-40. It can be observed that when comparing to the bio-graphite spectrum G band for GO shifted to 1590 cm^{-1} from the spectrum of graphite 1577 cm^{-1}. This is due to isolated double bonds resonating at a higher frequency than the G band of graphite, proving that the oxidation process took place (Xu et al., 2015). Id/Ig value for GO is higher than bio-graphite PKS-1300-40, 1.02 and 0.46, respectively, indicating higher defect structure related to extensive oxidation.

Figure 11 shows the Raman spectra of GO from OPF-1100-20 as a comparison with synthetic Bio-Graphite. A similar observation with the PKS spectrum is observed as the G band for GO shifted toward a higher wavenumber, indicating the oxidation of graphite-like material (Abdolhosseinzadeh et al., 2015; Nasir et al., 2017). As G-band shifted up due to a structural defect induced by the attachment of the oxygen-containing functional group to the basal plane of graphene during the oxidation of graphite. Consequently, leading to a higher Id/Ig value for GO than bio-graphite, 0.97 and 0.93, respectively.

Figure 12 shows the Raman spectra of GO Graphene Oxide and bio-graphite from the EFB sample. For GO, the G band has upshifted to 1592 $cm^{-1,}$ and the D band intensified due to the formation of oxygen functionalities, which correspond to defect sites created in graphite during oxidation (De Silva et al., 2018; Xu et al., 2015). Id/Ig value for GO was higher than bio-graphite 0.98 and 0.47, related to a higher amount of disordered and defective structure in GO proving a successful oxidation process took place. Due to the oxidation of graphite, the D band intensified, reflecting a reduction in the size of the order sp2 domain due to the attachment of the functional group. While the G band widened and shifted due to several factors, the most plausible factor is the generation of isolated double bonds on GO flakes that vibrate at a higher frequency than a double bond of graphite sheet.

Conclusions

In conclusion, the catalytic graphitization process with the addition of new Iron-Silica hybrid catalyst had successfully modified the lignocellulosic structure of PKS, EFB and OPF into highly crystalline graphitic carbon. These were evidenced by the appearance of a graphite diffraction peak at 2θ~26° observed in the XRD patterns for most of the samples and calculated interlayer spacing ranging from 0.3315 - 0.3335 nm and very close to the interlayer spacing of commercial graphite (0.3347 nm), proving the successful transformation of amorphous carbon into a highly graphitic structure. It is found that the degree of graphitization is affected by heat treatment temperature, amount of catalyst loading and type of raw materials. For heat treatment, temperature parameters PKS and EFB had been observed to achieve a high degree of graphitization at 1300℃, whereas for OPF, the highest degree of transformation was observed at 1100℃. Meanwhile, for the effect of catalyst loading, EFB showed the highest degree of graphitization at 60 wt. % Iron loading, but PKS revealed the optimum Iron loading would be either at 60 wt. % or 40 wt. % meanwhile, the highest degree of graphitization for OPF was observed at 20 wt. % catalyst loading. Both results show comparable observations to a previous study done by another author (Malas et al., 2017; Sharma et al., 2020; Xu et al., 2015). Overall it is found that Palm Kernel Shell is the greatest carbon precursor for the graphitization process, followed by EFB and OPF based on nearest interlayer spacing as compared to natural graphite standard, lowest Id/Ig value and HRTEM image of PKS-1300-40 sample. Overall, XRD and Raman structure of GO justified the bio-graphite is successfully transformed to Graphene oxide via the modified hummer method.

References

Abdolhosseinzadeh, S., Asgharzadeh, H., & Kim, H. S. (2015). Fast and fully-scalable synthesis of reduced graphene oxide. Scientific reports, 5(1), 1-7.

Adela, J., Ondrej, J., Zdenek, S. & David, S. (2022). Synthesis and Applications of Graphene Oxide. National Library of Medicine 15(3):920.

Artur T. Dideikin and Alexandar Y.Vul, Graphene Oxide and Derivatives: The Place in Graphene Family, Frontiers in Physics, Vol. 6, Article 149 Jan 2019.

De Silva, K. K. H., Huang, H. H., & Yoshimura, M. (2018). Progress of reduction of graphene oxide by ascorbic acid. Applied Surface Science, 447(March), 338– 346.

Dalton, O. S., Mohamed, A. F., & Chikere, A. O. (2017). Status Evaluation of Palm Oil Waste Management Sustainability in Malaysia. OIDA International Journal of Sustainable Development, 10(12), 41–48.

Hobart M King. (2015). Graphite. Geology.Com. https://geology.com/minerals/graphite.shtml

Hoekstra, J., Beale, A. M., Soulimani, F., Versluijs-Helder, M., Geus, J. W., & Jenneskens, L. W. (2015). Base metal catalyzed graphitization of cellulose: A combined Raman spectroscopy, temperature-dependent X-ray diffraction and high-resolution transmission electron microscopy study. Journal of Physical Chemistry C, 119(19), 10653–10661.

Ingrid, M., Michal, L and Stefan, J. (2000). The influence of microwave radiation on the failure of rocks. Acta Montanistica Slovaca, 5(3), 283-285.

Johnson, M. T., & Faber, K. T. (2011). Catalytic graphitization of three-dimensional wood-derived porous scaffolds. Journal of Materials Research, 26(01), 18–25.

Kamil, M., Zofia, K. and Henrieta, P. (2006). Utilization of wood waste in condition of Slovak Republic**.** Acta Montanistica Slovaca, 11(2), 137-143.

Kaniapan, S., Hassan, S., Ya, H., Nesan, K. P., & Azeem, M. (2021). The utilisation of palm oil and oil palm residues and the related challenges as a sustainable alternative in biofuel, bioenergy, and transportation sector: A review. Sustainability (Switzerland), 13(6).

Kim, T., Lee, J., & Lee, K. H. (2016). Full graphitization of amorphous carbon by microwave heating. RSC advances, 6(29), 24667-24674.

King, R. J. (2006). Minerals explained 43: Graphite. In Geology Today (Vol. 22, Issue 2, pp. 71–77). Blackwell Publishing Inc.

Khosroshahi, Z., Kharaziha, M., Karimzadeh, F., & Allafchian, A. (2018). Green reduction of graphene oxide by ascorbic acid. AIP Conference Proceedings, 1920.

Lim, Y., Chu, J. H., Lee, D. H., Kwon, S.-Y., & Shin, H. (2017). Increase in graphitization and electrical conductivity of glassy carbon nanowires by rapid thermal annealing. Journal of Alloys and Compounds, 702, 465–471.

Liu, Yang, Chen, J., Cui, B., Yin, P., & Zhang, C. (2018). Design and Preparation of Biomass-Derived Carbon Materials for Supercapacitors: A Review. C, 4(4), 53.

Lovás, M. et al., 2011. The application of microwave energy in mineral processing - a review, Acta Montanistica Slovaca, 16(2), 137-148.

Malas, A., Bharati, A., Verkinderen, O., Goderis, B., Moldenaers, P., & Cardinaels, R. (2017). Effect of the GO reduction method on the dielectric properties, electrical conductivity and crystalline behavior of PEO/rGO nanocomposites. Polymers, 9(11).

Mcallister, M. J., Li, J., Adamson, D. H., Schniepp, H. C., Abdala, A. a, Liu, J., Herrera-alonso, O. M., Milius, D. L., Car, R., Prud, R. K., & Aksay, I. a. (2007). Expansion of Graphite. Society, 19(4), 4396–4404.

Major, I., Pin, J.-M., Behazin, E., Rodriguez-Uribe, A., Misra, M., & Mohanty, A. (2018). Graphitization of Miscanthus grass biocarbon enhanced by in situ generated FeCo nanoparticles. 20, 2269.

Máté, D., Oláh, J., Laknern, Z., & Popp, J. (2017). Food chemistry patents influence on productivity: A case study of a sectoral approach in various OECD countries. Polish Journal of Management Studies, 16(2), 160-170.

Mohammad Padzil, F. N., Lee, S. H., Ainun, Z. M. A. ari, Lee, C. H., & Abdullah, L. C. (2020). Potential of oil palm empty fruit bunch resources in nanocellulose hydrogel production for versatile applications: A review. Materials, 13(5).

Mohammed, A.A.F & Yoshito, A. (2022). A route towards graphene from lignocellulosic biomass: Technicality, challenges, and their prospective applications. Journal of Cleaner Production 380. 135090

Mohd, M., Atirah, N., Hashim, N., Fikri, A., & Razif, M. (2020). Pulp and paper production from oil palm empty fruit bunches: A current direction in Malaysia. Journal of Agricultural and Food Engineering, 1(2), 1–9.

Nasir, S., Hussein, M., Yusof, N., & Zainal, Z. (2017). Oil Palm Waste-Based Precursors as a Renewable and Economical Carbon Sources for the Preparation of Reduced Graphene Oxide from Graphene Oxide. Nanomaterials, 7(7), 182.

Nettelroth, D., Schwarz, H. C., Burblies, N., Guschanski, N., & Behrens, P. (2016). Catalytic graphitization of ordered mesoporous carbon CMK-3 with iron oxide catalysts: Evaluation of different synthesis pathways. Physica Status Solidi (A) Applications and Materials Science, 213(6), 1395–1402.

Paulchamy B., Arthi G and Lignesh B.D. (2015). A Simple Approach to Stepwise Synthesis of Graphene Oxide Nanomaterial. Journal of Nanomedicine & Nanotechnology 6 : 253.

Plewa, A. (2019). Asphalt mixtures with binders fluidized by addition of vegetable origin oil for applications as flexible anti-crack layers. Roads and Bridges - Drogi i Mosty, 18(3), 181-192.

Poh, H. L., Šaněk, F., Ambrosi, A., Zhao, G., Sofer, Z., & Pumera, M. (2012). Graphenes prepared by Staudenmaier, Hofmann and Hummers methods with consequent thermal exfoliation exhibit very different electrochemical properties. Nanoscale, 4(11), 3515–3522.

Qiu, T., Yang, J., & Bai, X. (2019). Environmental Effects Investigation on microstructural changes of Anthracite during Graphitization and effect of Silica content on product crystal structure. Energy Sources, Part A: Recovery, Utilization, and Environmental Effects, 0(0), 1–14.

Salvador, F., Alfonso, M., Edgar, C., Claudia, Y.M. and Uriel, S. (2019). Asphalt as raw material of graphene-like resources. Fuel (241), 297-303.

Sankar, S., Ahmed, A. T. A., Inamdar, A. I., Im, H., Im, Y. Bin, Lee, Y., Kim, D. Y., & Lee, S. (2019). Biomass-derived ultrathin mesoporous graphitic carbon nanoflakes as stable electrode material for high-performance supercapacitors. Materials & Design, 169, 107688.

Serrano-Ruiz, J. C., West, R. M., & Dumesic, J. A. (2010). Catalytic Conversion of Renewable Biomass Resources to Fuels and Chemicals. Annual Review of Chemical and Biomolecular Engineering, 1(1), 79–100.

Sevilla, M., & Fuertes, A. B. (2010). Graphitic carbon nanostructures from cellulose. Chemical Physics Letters, 490(1–3), 63–68.

Sevilla, M., Sanchís, C., Valdés-Soh, T., Morallón, E., & Fuertes, A. B. (2007). Synthesis of graphitic carbon nanostructures from sawdust and their application as electrocatalyst supports. Journal of Physical Chemistry C, 111(27), 9749–9756.

Sharma, N., Arif, M., Monga, S., Shkir, M., Mishra, Y. K., & Singh, A. (2020). Investigation of bandgap alteration in graphene oxide with different reduction routes. Applied Surface Science, 513(October 2019), 145396.

Srinivasan, P., Sarmah, A. K., Smernik, R., Das, O., Farid, M., & Gao, W. (2015). A feasibility study of agricultural and sewage biomass as biochar, bioenergy and biocomposite feedstock: Production, characterization and potential applications. Science of the Total Environment, 512–513, 495–505.

Xia, J., Zhang, N., Chong, S., Li, D., Chen, Y., & Sun, C. (2018). Three-dimensional porous graphene-like sheets synthesized from biocarbon via low-temperature graphitization for a supercapacitor. Green Chemistry, 20(3), 694–700.

Xu, C., Shi, X., Ji, A., Shi, L., Zhou, C., & Cui, Y. (2015). Fabrication and characteristics of reduced graphene oxide produced with different green reductants. PLoS ONE, 10(12).

Zoraida, G., Beatriz, A., Georgeta, P., Sorin, M.A., Marius, F.D., Valerica, S., Juan, J.F., Marcos, G., Grazyna, G. and Sonia, M.E. (2021). Graphene materials from microwave-derived carbon precursors. Fuel Processing Technology. 217.